Coefficient difference based watermark detector in nonsubsampled contourlet transform domain

Xiang-yang Wang [a,*], Si-yu Zhang [a], Tao-tao Wen [a], Hong-ying Yang [a], Pan-pan Niu [a,b]

[a] *School of Computer and Information Technology, Liaoning Normal University, Dalian 116029, PR China*
[b] *Guangdong Key Laboratory of Intelligent Information Processing and Shenzhen Key Laboratory of Media Security, Shenzhen 518060, PR China*

ARTICLE INFO

ABSTRACT

Imperceptibility and robustness are two main requirements of any image watermarking systems to guarantee desired functionalities, but there is a tradeoff between them from the information–theoretic perspective. It is a challenging work to design a high performance digital watermarking scheme to keep a trade-off between imperceptibility and robustness. By modeling the nonsubsampled Contourlet transform (NSCT) coefficient differences with ranked set sample (RSS) based Cauchy distribution and employing locally most powerful (LMP) test, we propose a locally optimum image watermark detector in NSCT domain. In the proposed scheme, we first compute the robust coefficient differences according to the inter-scale dependency between NSCT coefficients, and then embed the digital watermark into the significant NSCT coefficient difference subband. At the watermark receiver, robust NSCT coefficient differences are firstly modeled by employing the Cauchy distribution, where the statistical properties of NSCT coefficient differences are captured accurately. Then the RSS approach is introduced to estimate the location parameter and shape parameter of Cauchy distribution. And finally an optimal detector for multiplicative watermarking is developed using the LMP decision rule and RSS-based Cauchy distribution. Also, we utilize the statistical model to derive the closed-form expressions for the watermark detector. Experimental results demonstrate the high efficiency of our watermarking scheme, which can provide better imperceptibility and outstanding robustness against various attacks, in comparison with the state-of-the-art approaches recently proposed in the literature.

© 2019 Published by Elsevier Inc.

1. Introduction

WITH the rapid growth and widespread use of Internet and multimedia technology, there is an urgent need for intellectual-property protection of digital multimedia. Digital watermarking systems have been proposed as a possible and efficient answer to the problem of copyright protection of digital data [16,17]. Whilst digital watermarking can be widely applied to various digital media, such as audio, video or image, and this paper focuses on digital image watermarking. Generally, imperceptibility and robustness are two main requirements of any image watermarking systems to guarantee desired

---

functionalities, but there is a tradeoff between them from the information–theoretic perspective. Imperceptibility denotes the ability of embedding the watermarks without significantly lowering the image quality. Robustness denotes the capability of extracting the watermarks under various attacks. The above two requirements are equally important for an image watermarking scheme, but there is an ambivalence between them. Improving the ability of robustness and imperceptibility simultaneously has long been a challenging open issue [22].

In the past decades, in order to work out effectively the tradeoff between the imperceptibility and robustness of the watermark data, the statistical properties of the transform coefficients have received great attention, and some statistical modeling-based transform domain multiplicative watermarking schemes have been proposed, which take advantage of the Human Visual System (HVS) properties. Up to now, the usually adopted transforms are Discrete Fourier transform (DFT) [5], Discrete Cosine transform (DCT) [6,12], Discrete wavelet transform (DWT) [18,29], Curvelet transform [13], Ridgelet transform [20], Shearlet transform [1], Contourlet transform [23,25], and Nonsubsampled Shearlet transform (NSST) [30]. The commonly used statistical models include Gauss–Hermite expansion [24], Generalized Gaussian distribution(GGD) [19], Normal Inverse Gaussian (NIG) distribution [26], Alpha-stable distribution [25], Hidden Markov Model (HMM) distribution [4], and Bessel-K form (BKF) distribution [7,23]. The ordinarily employed decision rules are Likelihood ratio test (LRT) [8], Generalized likelihood ratio test (GLRT) [28], Bayesian log-likelihood ratio test (LLRT) [27], the Rao test [9,18,21], Maximum likelihood (ML) test [7], and locally most powerful (LMP) test [29].

The performance of a statistical model-based watermark detector is highly influenced by the accurate modeling of robust transform coefficients. The existing statistical model-based watermarking approaches all employed directly the transform coefficients to insert watermark signal and design watermark detector. However, it is shown that the NSCT coefficient differences from the adjacent scale always offer higher robustness, which is more suitable for embedding watermark information and developing watermark detector. In this paper, by modeling the robust NSCT coefficient differences with ranked set sample (RSS) based Cauchy distribution and employing LMP decision criterion, we design a locally optimal image watermark detector in NSCT domain. The novelty of the proposed scheme is that (1) Robust NSCT coefficient differences are employed to insert watermark signal and design watermark detector; (2) The RSS-based Cauchy distribution is introduced to capture effectively the statistical behavior of robust NSCT coefficient differences; (3) A blind locally optimum NSCT domain multiplicative detector is designed using locally most powerful test criterion, which is optimal for non-Gaussian weak watermark signals in the sense of minimizing detection errors.

This paper is organized as follows. In Section 2, a review of previous related works is presented. In Section 3, we briefly introduce NSCT and the NSCT coefficient differences. Also, we investigate the robustness of the NSCT coefficient differences by subjective visual error and MSE terms. In Section 4, we describe the statistical modeling of the NSCT coefficient differences using RSS-based Cauchy distribution. Section 5 provides the proposed multiplicative watermarking approach in the NSST domain. In Section 6, a blind locally optimum NSCT domain multiplicative detector is developed using RSS-based Cauchy PDF and LMP test. Experimental results are provided to prove the outstanding performance of the proposed scheme in Section 7. Finally, Section 8 concludes this paper.

2. Related work

In general, the main objective of developing an effective image watermarking technique is to satisfy both imperceptibility and robustness requirements, but there is contradiction between these two aspects. To achieve this objective, the statistical properties of the transform coefficients have received a lot of attention, and there have been many efforts in developing statistical modeling-based transform domain multiplicative watermarking approaches.

Barni et al. [5] provided an optimum multiplicative watermark detector in the DFT domain using the Weibull distribution, in which the work performance of the watermark detector was evaluated by Monte Carlo simulations. Briassouli et al. [6] proposed a novel approach to the watermark detection problem for still images in the DCT domain, which employed locally optimum and nonlinear detectors. Bi et al. [9] presented a RAO hypothesis detector by modeling Cauchy distribution for the nonsubsampled contourlet transform subband coefficients in the field of additive spread spectrum image watermarking. But, they all embedded simply the watermark message into the transform coefficients of an image, which are always fragile to various attacks. The adopted maximum likelihood estimators (MLEs) are usually biased in the case of the finite sample size. Besides, the RAO test can show an asymptotically optimal performance only when the number of data samples is large, the prior probability distribution function of the signal is known, and the signal to be detected is weak. However, when the embedded watermarks are relatively strong, it usually has lower detection efficiency. Wang et al. [29] employed generalized Gaussian distribution to model DWT coefficients, and proposed a locally optimum watermark detector based on a locally most powerful test. But, GGD is not a suitable PDF for capturing the statistical properties of the DWT coefficients. Rahman et al. [24] proposed an image watermark detector in DWT domain, wherein a PDF based on the Gauss–Hermite expansion and the log-likelihood ratio test are employed. Kwitt et al. [18] proposed a DWT domain watermark detector using a RAO decision rule, in which the generalized Gaussian distribution and Cauchy distribution are used to model DWT coefficients. However, the RAO test can show an asymptotically optimal performance only when the number of data samples is large, the prior probability distribution function of the signal is known, and the signal to be detected is weak. Bian et al. [7] designed a DWT domain digital watermark detector, in which the likelihood ratio test and Bessel K form (BKF) probability density function are used. Bian et al. [8] presented a locally optimal watermark detection based on the wavelet domain, wherein

the Bessel K Form distribution is utilized. The proposed detector is suitable for the watermark detection, but it only has superior performance when the strength of watermark is very weak.

Sadreazami et al. [25] proposed a new multiplicative watermarking approach in the Contourlet domain, in which the alpha-stable statistical distributions and the likelihood ratio test are employed. Amirmazlaghani et al. [2] modeled the DWT coefficients with Gaussian Mixture Model (GMM), and proposed a DWT domain multiplicative watermark detector based on maximum likelihood decision rule. The proposed GMM detector is suitable for the watermark detection, but the computation of the detection response is computationally more expensive than the estimation procedure. Sadreazami et al. [27] employed the multivariate Cauchy distribution for fitting the Contourlet coefficients, and presented a multiplicative image watermark detector based on Bayesian log-likelihood ratio test. Amini et al. [3] developed a multiplicative image watermarking scheme in the wavelet domain, where the vector-based hidden Markov model and log-likelihood ratio test are employed. Rabizadeh et al. [23] used the BKF statistical distribution to model Contourlet coefficients, and developed a Contourlet domain multiplicative watermark detector using ML decision rule. Sadreazami et al. [26] modeled the Contourlet coefficients with normal inverse Gaussian (NIG) distribution, and introduced a multiplicative image watermark decoder using the maximum likelihood decision. Dong et al. [12] introduced a maximum-likelihood detection for DCT domain watermarking schemes, in which the Weibull distribution is utilized to model the DCT AC and DC coefficients. Santhi et al. [28] used DWT and DCT techniques to obtain the frequency components, and then proposed a hybrid domain image watermark detector using the Weibull distribution and Generalized likelihood ratio test. Amini et al. [4] employed the vector-based hidden Markov model (HMM) to capture the distribution of the wavelet coefficients, as well as proposed a locally optimal DWT domain watermark detector based on the Neyman–Pearson test. Bhinder et al. [10] designed a DWT domain digital watermark detection using Gaussian distribution and maximum likelihood decision rule. Etemad et al. [14] used t-location scale distribution to model Contourlet coefficients, and developed a Contourlet domain multiplicative watermark detector using t-location scale distribution and likelihood ratio decision rule. However, the watermark capacity in the scheme is limited.

3. Coefficient difference in NSCT domain

3.1. Nonsubsampled contourlet transform (NSCT)

Contourlet transform (CT) provides a real sparse method for 2-D image. CT is composed by combining the Laplacian Pyramid (LP) decomposition and the directional filter bank (DFB). Compared with other wavelet transform, CT also provides multi-scale and directional image representation. However, the LP filter used in the CT construction contains the down-samplers process. So the CT is not shift-invariant. But shift-invariant is crucial for image processing. It is proposed in [11] that the basis function of CT is not sufficiently localization in the frequency domain. Spectral aliasing phenomenon exists between the direction subbands. This may lead to the same direction information simultaneously appears in different direction subbands and greatly reduce the direction of selectivity. In order to overcome the phenomenon of spectral aliasing, and enhance the shift-invariance and direction selectivity, Cunha et al. [11] proposed the Nonsubsampled Contourlet transform (NSCT).

NSCT is based on CT. Compare with CT, the main difference is that NSCT cancels the down-samplers and up-samplers during the image decomposition and reconstruction. The NSCT has been improved not only to maintain the properties of multi-scale and multidirectional of CT, but also possess the shift-invariant which CT does not have. The NSCT construction can be decomposed into two parts: Nonsubsampled Pyramid (NSP) and Nonsubsampled Directional Filter Bank (NSDFB). Firstly, in order to achieve multi-scale decomposition, the original image is decomposed by the NSP into a low frequency image and many high frequency images. Secondly, in order to achieve multi-directional decomposition, high frequency images of each scale are decomposed by NSDFB with l stages, furthermore producing 2^l directional subbands with wedge-shaped frequency partition. In view of this, different scale and different direction subbands images can be obtained.

Fig. 1(a) shows the standard gray image "Lena" and Fig. 1(b)–(d) show its NSCT representation. In this particular decomposition, the image is divided into an approximation image and two detail scales, and each detail scale is further partitioned into four directional subbands.

3.2. NSCT coefficient difference

Up to now, almost all image watermarking algorithms embed or detect watermark information by employing directly the pixel values or transform coefficients, which always shows low robustness against various attacks. In this paper, we will use the robust NSCT coefficient difference [11,31] to embed and detect digital watermark.

Suppose that the original image are decomposed by the NSCT up to scale s (in this paper, s=2), and four directions are employed in each decomposition scale, as shown in Fig. 1(a)–(d). Then, at each scale, four directional subbands are generated, and the NSCT coefficients of four directional subbands at scale 2 and scale 1 are computed and denoted by $F_j(x, y)$ and $S_j(x, y)$ respectively, where $j = 1, 2, \cdots, 4$ denotes decomposition directions. The NSCT coefficient difference of directional subbands $F_j(x, y)$ and $S_j(x, y)$ can be calculated over their NSCT domains using their coefficient difference of two subband coefficients as

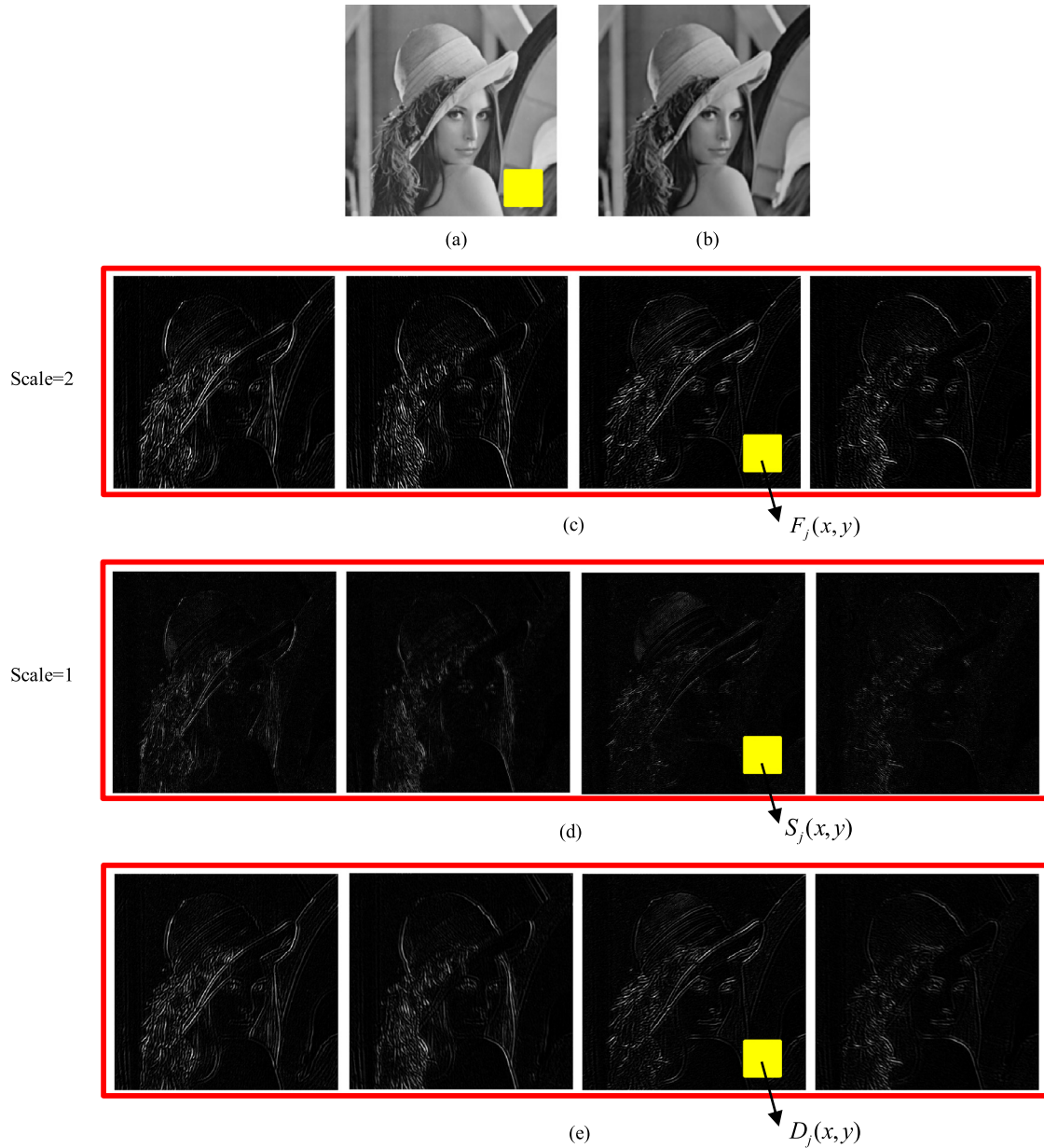$$D_j(x, y) = F_j(x, y) - S_j(x, y) \tag{1}$$

Fig. 1. The NSCT representation of the standard gray image Lena: (a) Original Lena, (b) Lowpass subband, (c) Highpass subbands at scale 2, (d) Highpass subbands at scale 1, (e) NSCT coefficient difference subband.

where $1 \leq x \leq M$, $1 \leq y \leq N$, and $M \times N$ denotes image size. The NSCT coefficient difference $\{D_j(x, y)\}$ can be viewed as a two-dimensional (2-D) random field. For ease of mathematical notation, D_j is used to represent the entire random field, while $D_j(x, y)$ denotes a specific value at the location of (x, y), as shown in Fig. 1(e).

Fig. 2 shows the visible differences between original image and the attacked image, original highpass subband at scale 2 and the attacked one, original highpass subband at scale 1 and the attacked one, and original NSCT coefficient difference subband and the attacked one, under various attacks, respectively. Also, we use MSE (Mean squared error) to evaluate the robustness of signal, which denotes the mean squared-error between the original signal and the attacked one. The smaller MSE value means the smaller error or differences between original signal and the attacked one. Namely, the smaller MSE value means that the original signal is more robust to various attacks. Table 1 shows the MSEs between original image and the attacked image, original highpass subband at scale 2 and the attacked one, original highpass subband at scale 1 and the attacked one, and original NSCT coefficient difference subband and the attacked one, for standard gray images Lena, Barbara, Peppers under various attacks, respectively.
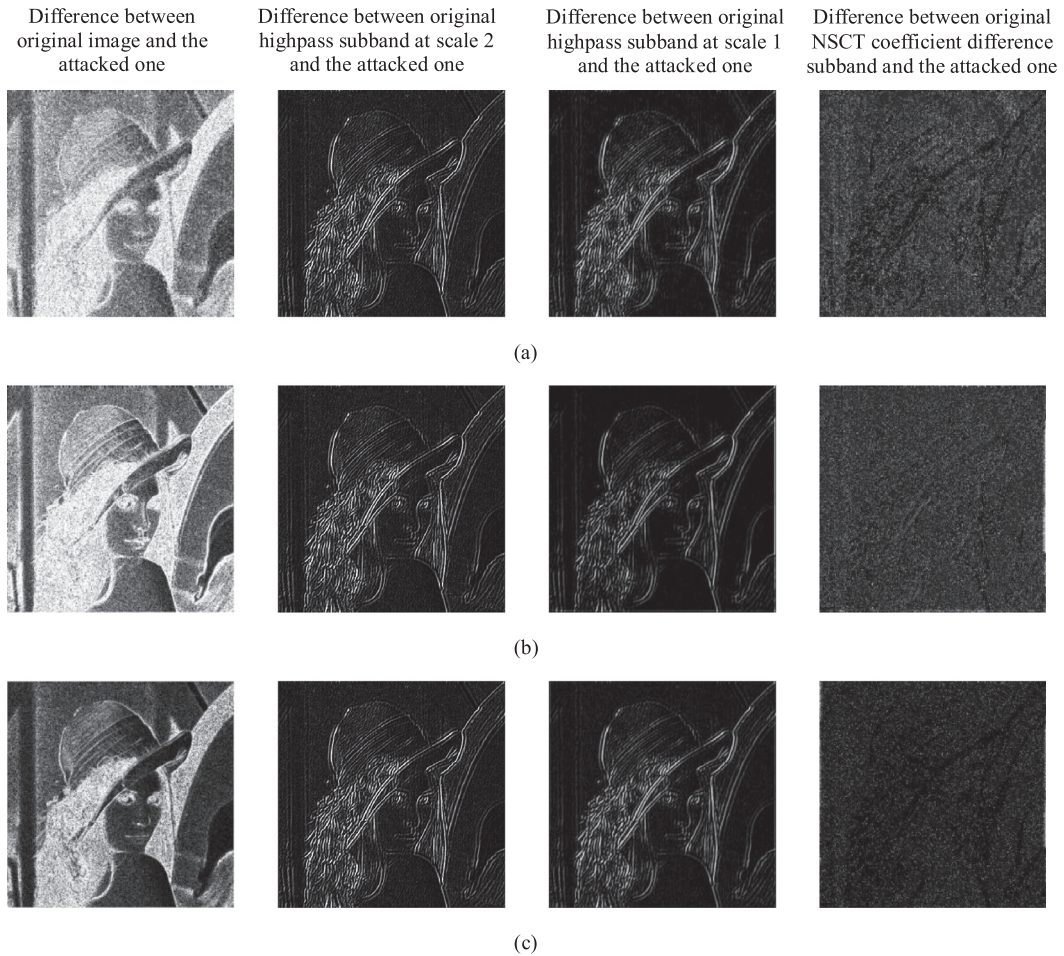
(a)

(b)

(c)

Fig. 2. The visible differences between original image and the attacked image, original highpass subband at scale 2 and the attacked one, original highpass subband at scale 1 and the attacked one, and original NSCT coefficient difference subband and the attacked one, under various attacks, respectively. (a) JPEG 30, (b) Median filtering (3×3), (c) Salt and peppers noise (0.01).

Table 1
MSEs between original signal and the attacked one (Best results are shown in bold).

| Original signal and the attacked one	Lena			Barbara			Pepper		
	JPEG 30	Median filtering (3 × 3)	Salt and peppers noise (0.01)	JPEG 30	Median filtering (3 × 3)	Salt and peppers noise (0.01)	JPEG 30	Median filtering (3 × 3)	Salt and peppers noise (0.01)
Original image and the attacked one	24.3114	77.7641	4.8841	61.6234	287.3976	28.0977	28.3295	89.3422	6.4671
Original highpass subband at scale 2 and the attacked one	1.6986	8.4305	0.4476	1.9102	10.6510	0.6994	3.9372	6.9225	1.0272
Original highpass subband at scale 1 and the attacked one	4.9980	10.5903	0.9137	6.7536	12.7204	1.3248	4.9876	7.2537	1.2539
Original NSCT coefficient difference subband and the attacked one	**0.8785**	**1.0470**	**0.2686**	**1.6044**	**1.3488**	**0.4029**	**1.4623**	**4.5999**	**0.3409**
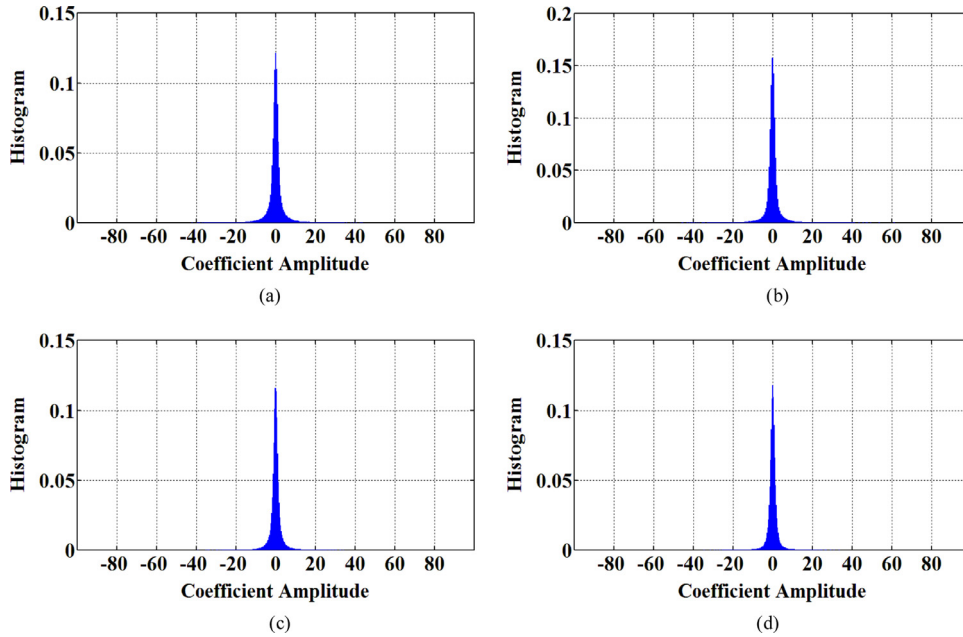
Fig. 3. The histograms of NSCT difference coefficients for four subbands as shown in Fig. 1(e). The kurtosis values of the distributions are measured at: (a) 17.6606, (b) 22.0900, (c) 18.1745, and (d) 19.4919.

From Fig. 2 and Table 1, we can see that NSCT coefficient difference is more robust than pixel value or transform coefficient, so we employ the NSCT coefficient difference to embed and detect digital watermark in this paper.

3.3. Marginal statistics of NSCT coefficient difference

It is very important to analyze fully the marginal statistics of signal for signal modeling. In this subsection, we employ the standard grayscale images from Computer Vision Group Test Images database to analyze the statistical properties of the NSCT coefficient difference. Here, we analyze the marginal statistics of NSCT coefficient difference by fusing the distribution histogram and kurtosis value. Fig. 3 provides the histograms of NSCT difference coefficients for four NSCT coefficient difference subbands, as shown in Fig. 1(e). We can easily observe from the Fig. 3 that there presents a sharp peak close to zero as well as heavy tails in both sides. Namely, the vast majority of NSCT difference coefficients are around zero. Next, we further calculate the kurtosis values of the histograms as can be seen in Fig. 3, which are 17.6606, 22.0900, 18.1745, and 19.4919, respectively. These kurtosis values are all much higher than 3, and we know that the standard kurtosis value of Gaussian distribution is equal to 3. Therefore, the NSCT difference coefficients are obviously highly non-Gaussian. Further, we need to find a more suitable statistical distribution for the NSCT coefficient difference modeling.

4. RSS-based Cauchy modeling of NSCT coefficient difference

4.1. Cauchy distribution model

Employing a suitable statistical distribution to model the NSCT coefficient difference can effectively improve the detection accuracy of the watermark detector. We employ the RSS-based Cauchy distribution to fit the NSCT coefficient differences in this paper.

Cauchy is an essential member of the family of symmetric alpha-stable ($S\alpha S$) distributions. In addition, Cauchy is the only member of the family with a closed-form expression for the probability density function (PDF). The standard PDF of the Cauchy distribution with location parameter $-\infty < \delta < \infty$ and shape parameter $\gamma > 0$ is given by

$$p(x|\gamma, \delta) = \frac{1}{\pi} \frac{\gamma}{\gamma^2 + (x - \delta)^2} \tag{2}$$

with $-\infty < x < \infty$. The Cauchy distribution is different from the Gaussian distribution, its PDF decays at a slower rate. This makes the Cauchy have strong descriptive ability to model the heavy tailed distribution. Therefore, the Cauchy distribution is particularly suitable to model the NSCT coefficient differences.

Parameter estimation is of significant for modeling NSCT coefficient differences. But for Cauchy distribution, we cannot employ the conventional methods, including the maximum likelihood estimator (ML), the least squares estimator (LS), and

Table 2
The Kolmogorov–Smirnov performance comparisons of various statistical models (Best results are shown in bold).

Test image	Direction	Weibull distribution	Exponential distribution	General Gaussian distribution	Rayleigh distribution	Laplacian distributions	BKF distribution	RSS-based Cauchy distributions
Lena	1	0.0587	0.1101	0.1405	0.4787	0.3445	0.1753	**0.0176**
	2	0.0628	0.1049	0.1569	0.4823	0.3190	0.2432	**0.0220**
	3	0.0493	0.0812	0.1665	0.4388	0.2764	0.2135	**0.0243**
	4	0.0438	0.0576	0.1882	0.4021	0.2258	0.2589	**0.0338**
Barbara	1	0.0622	0.1789	0.0787	0.5533	0.5124	0.1805	**0.0091**
	2	0.0525	0.1305	0.0924	0.5022	0.4253	0.1765	**0.0148**
	3	0.0422	0.0817	0.1379	0.4431	0.3050	0.2486	**0.0250**
	4	0.0362	0.0661	0.1362	0.3977	0.2824	0.1501	**0.0256**
Peppers	1	0.0486	0.0609	0.1138	0.4106	0.2861	0.2488	**0.0361**
	2	0.0463	0.0546	0.1201	0.3971	0.2665	0.2692	**0.0388**
	3	0.0475	0.0570	0.1356	0.4017	0.2586	0.2791	**0.0381**
	4	0.0457	0.0598	0.1307	0.4155	0.2723	0.2725	**0.0361**
Average		0.0497	0.0869	0.1331	0.4436	0.3145	0.2264	**0.0268**

the moment based method (MM), to estimate accurately the model parameters. This is because that: First, The high-order moment, variance, and mathematical expectation of Cauchy distribution do not exist, so we cannot employ directly the MM approach or LS method to estimate the model parameters of Cauchy distribution. Second, ML method is straightforward and effective statistical parameter estimation, moreover, it often needs to select parameter values that offer the highest value of the likelihood function by computing the root of the derivative of the likelihood function. But when the random variable follows a Cauchy distribution, we always cannot obtain the optimal analytic solution of the likelihood function, hence the numerical solution of the likelihood function results in lower parameter estimation accuracy.

In this paper, we introduce the Ranked set sample (RSS) approach [32] for estimating the model parameters of Cauchy distribution. The RSS-based Cauchy parameter estimation approach has the following advantages: (1) the higher estimation precision can be obtained when the larger sample size is employed, (2) the relatively high estimation precision can also be obtained when the sample size is small (The relative error can be less than 0.002), (3) when the sample size remain unchanged, the estimation precision is related to location parameter δ, and the estimation precision declines gradually with the increasing of location parameter δ. For RSS-based Cauchy parameter estimation, the two-parameter Cauchy distribution function is defined as $Cauchy(\gamma, \delta)$, and the random variable following the Cauchy distribution is denoted as $\xi \sim Cauchy(\gamma, \delta)$, so the cumulative distribution function $F(x)$ of ξ can be expressed as follow

$$F(x) = \frac{1}{2} + \frac{1}{\pi} \arctan \frac{x - \gamma}{\delta} \tag{3}$$

where $-\infty < x < +\infty$, $-\infty < \gamma < +\infty$, $\delta > 0$. $F_\xi(\gamma) = \frac{1}{2}$ indicates that γ is the middle point of $Cauchy(\gamma, \delta)$, and $F_\xi(\gamma + \delta) = \frac{3}{4}$ indicates that $\gamma + \delta$ is the $\frac{3}{4}$ quantile of $Cauchy(\gamma, \delta)$, from which we can obtain the estimation values of γ and δ. Let $X_{n\frac{1}{2}}$ and $X_{n\frac{3}{4}}$ be the median and $\frac{3}{4}$ quantile of the sample respectively, then $X_{n\frac{1}{2}}$ and $X_{n\frac{3}{4}}$ can be used as γ and $\gamma + \delta$ of the parameter estimation.

4.2. RSS-based Cauchy modeling of NSCT coefficients differences

Cauchy distribution has been verified the most suitable to fit the heavy-tailed distribution. The NSCT coefficients differences can be modeled by using the Cauchy PDF in this paper, where the RSS approach is used to estimate the statistical parameters γ and δ.

Kolmogorov–Smirnov (KS) test is one of the powerful tools that can be used to examine the statistical features of signal. And in this paper, we utilize the KS metric to verify the excellent performance of the Cauchy statistical distribution. The KS metric can be expressed as follow

$$Q_{ks} = \max_{w \in R} |C_h(w) - C_e(w)| \tag{4}$$

where $C_h(w)$ and $C_e(w)$ indicate the cumulative distribution function (CDF) of the prior PDF as well as empirical data, respectively, the smaller Q_{ks} value means the superior modeling performance.

Here, we employ three standard gray images Lena, Barbara, and Peppers to test the modeling ability of the RSS-based Cauchy distribution on the NSCT coefficient differences. First, each test image is decomposed by the NSCT up to scale s (in this paper, $s = 2$), and four directions are utilized in each decomposition scale. Second, the NSCT coefficient difference subbands in four composition directions are obtained using Eq. (1). Then, we calculate the KS metric with different statistical distributions by selecting the NSCT coefficient difference subbands for each test image. Table 2 provides the KS metric results for various statistical distributions of the NSCT coefficient difference subbands. It can be seen from Table 2 that, the RSS-based Cauchy distribution is significantly superior to other statistical distribution models.
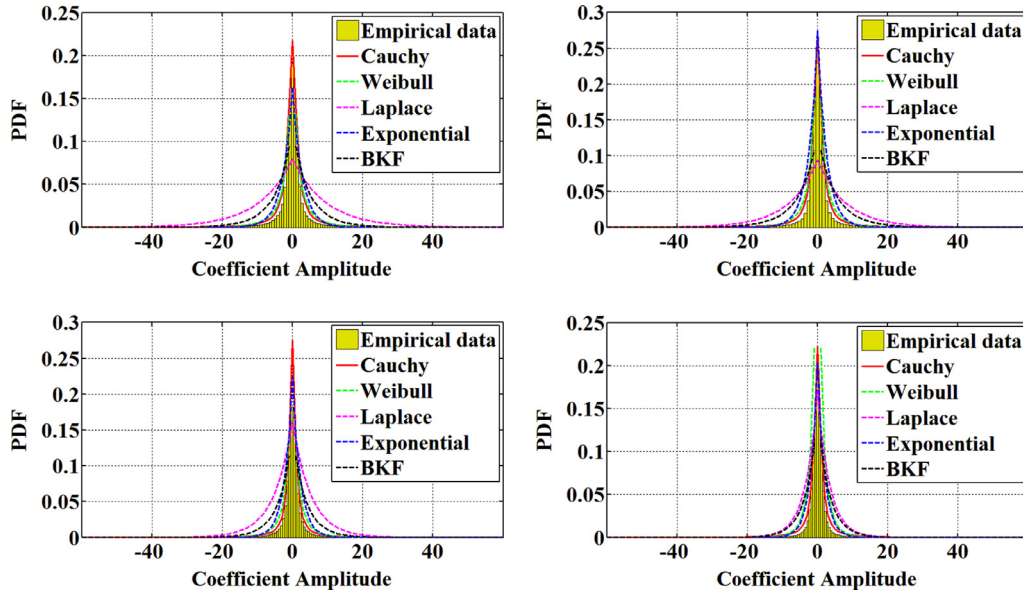
Fig. 4. The histograms of the actual data and the PDFs of different statistical models (for four NSCT coefficient difference subbands, as shown in Fig. 1(e)).

In order to prove that NSCT coefficient differences distribution can be fitted exactly by Cauchy PDF, we not only provide the histograms of the actual data, but also provide the PDFs of different statistical models, as can be seen in Fig. 4. From Fig. 4, it can be seen that the NSCT coefficients differences have distinct non-Gaussian properties, and the Cauchy statistical model can more accurately fit the NSCT coefficient differences distribution.

5. Digital watermark embedding

Imperceptibility and robustness are two main requirements of any image watermarking schemes to guarantee desired functionalities, but there is a tradeoff between imperceptibility and robustness from the information–theoretic perspective. To maintain simultaneously the imperceptibility and robustness, the watermark power ought to be proportional to the corresponding host image features, and multiplicative watermarking technique can be employed to implement this principle. It is quite difficult to observe due to interference proportional to the signal strength. Multiplicative watermarking techniques can always achieve more powerful watermark inserting while maintaining the watermarked image quality at an acceptable level. Furthermore, multiplicative watermarking approach is usually utilized based on the transform-domain for employing fully the HVS properties. In this paper, we adopt the multiplicative way to embed the watermark information into robust NSCT coefficient differences.

For our NSCT coefficient difference by using multiplicative watermarking algorithm, the digital watermark is inserted efficiently into the significant NSCT coefficient differences. For this purpose, NSCT is firstly performed on the original host image with the same direction numbers in each decomposition scale. The NSCT coefficient differences are then computed by using adjacent father and son NSCT coefficients at the same direction. And finally, NSCT coefficient difference blocks with the highest entropy are selected from the significant NSCT coefficient difference subband, and the watermark is inserted by modifying the significant NSCT coefficient differences using multiplicative approach.

Assuming that $I = \{f(x, y), 1 \leq x \leq M, 1 \leq y \leq N)\}$ indicates the original host image, and (x, y) represents the position of pixel. $W = \{w_l \in \{+1, -1\}, 1 \leq l \leq L\}$ denotes the watermark signal, which is generated by a pseudorandom sequence generator. Fig. 5 gives the flowchart of the proposed multiplicative watermark embedding procedure, and the corresponding watermark embedding process is summarized as follows.

Step 1: Nonsubsampled contourlet transform (NSCT). NSCT is performed on the original host image I with the same direction numbers in each decomposition scale. In this paper, two-scale NSCT is performed on the original host image with four directions in each decomposition scale, then the NSCT coefficients $F_j(x, y)$ and $S_j(x, y)$ of four directional subbands at scale two and scale one are obtained, respectively, where $j = 1, 2, \cdots, 4$ denotes decomposition directions.

Step 2: NSCT coefficient differences computing. The NSCT coefficient differences $D_j(x, y)$ of adjacent father directional subband coefficients $F_j(x, y)$ and son directional subband coefficients $S_j(x, y)$ are computed as

$$D_j(x, y) = F_j(x, y) - S_j(x, y)$$

where $1 \leq x \leq M$, $1 \leq y \leq N$, $M \times N$ denotes image size, and $j = 1, 2, \cdots, 4$ denotes decomposition directions.
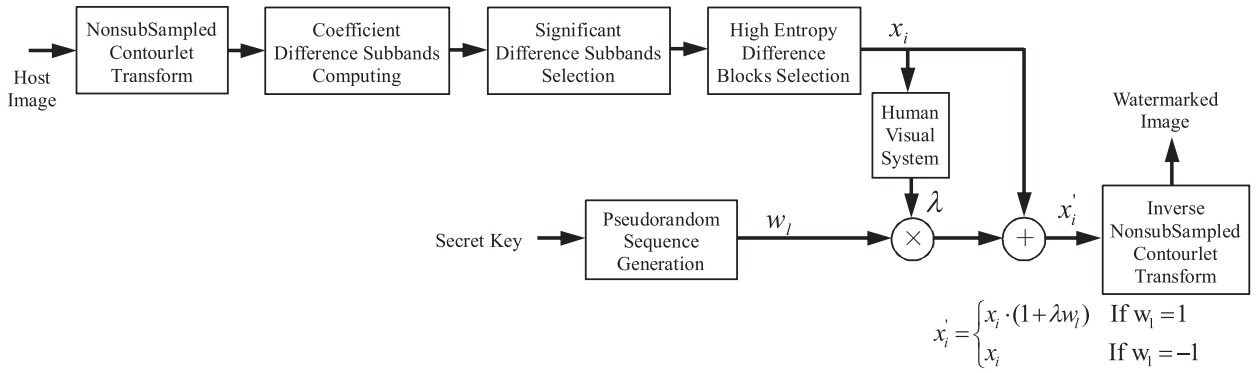
Fig. 5. The key components of the proposed multiplicative watermark embedding.

Step 3: Significant NSCT coefficient difference subband selection. We employ the multiplicative approach to embed digital watermark into robust NSCT coefficient difference subband. Furthermore, to enhance the watermark robustness, we embed the watermark data into the significant NSCT coefficient difference subband, for the significant NSCT coefficient difference subband usually has stronger ability to capture the robust image features than others. In this paper, we compute the energy of each NSCT coefficient difference subband, and then select the most significant one with the highest energy for watermark inserting. The most important NSCT coefficient difference subband can be computed as follows

$$d = \arg \max_{j} \left(\sum_{x} \sum_{y} \left(D_j[x, y] \right)^2 \right) \tag{5}$$

Step 4: Important subband blocking and high entropy blocks selection. HVS properties should be exploited fully to improve imperceptibility of proposed multiplicative watermarking, and the human eye is less sensitive to the image contents with high entropy values. For this purpose, we divided the significant NSCT coefficient difference subband into no-overlapping NSCT coefficient difference blocks, and then select L high entropy NSCT coefficient difference blocks $B_l(l = 0, 1, \ldots, L - 1)$ for embedding watermark.

Step 5: Watermark embedding. In this paper, we embed watermark bit w_l into the selected high entropy NSCT coefficient difference blocks $B_l(l = 0, 1, \ldots, L - 1)$ by modifying the NSCT coefficient differences, the watermark embedding rule can be derived as follow

$$x'_i = \begin{cases} x_i \cdot (1 + \lambda w_l) & \text{If watermark bit } w_l = 1 \\ x_i & \text{If watermark bit } w_l = -1 \end{cases}, \quad x_i \in B_l \tag{6}$$

$$fx'_i = fx_i + {x'_i}/{2}, \quad sx'_i = sx_i - {x'_i}/{2}$$

where x_i denotes the host NSCT coefficient differences, x'_i denotes the watermarked NSCT coefficient differences. fx_i and fx'_i are the corresponding host NSCT coefficients as well as watermarked NSCT coefficients of the father directional subband. sx_i and sx'_i are the corresponding host NSCT coefficients as well as watermarked NSCT coefficients of the son directional subband. B_l is the selected high entropy NSCT coefficient difference blocks. λ represents the watermark embedding strength, which is determined by the watermark to document ratio (WDR) given

$$WDR = 10 \log \left(\frac{\lambda^2}{\sigma_{x_i}^2} \right) \tag{7}$$

where the term "document" indicates the NSCT coefficient differences of the original host image, $\sigma_{x_i}^2 = \frac{1}{N} \sum_i x_i^2$ represents the variance of the host NSCT coefficient differences, N denotes the number of NSCT coefficient differences. In view of this, the digital watermark can be adapted to the local image properties of the original host.

Step 6: Inverse nonsubsampled contourlet transform (NSCT). In the last step, the watermarked image can be obtained by performing the inverse NSCT on the unchanged and watermarked NSCT coefficient differences.

6. Digital watermark detection

Usually, a digital watermarking approach for image copyright protection has an inserted digital watermark in the image works, and the watermark information is known to the intended receiver. So, the test of watermark existence, i.e., the detection of the watermark signal, is enough for the purpose of verifying the authenticity of an image. In this work, by modeling
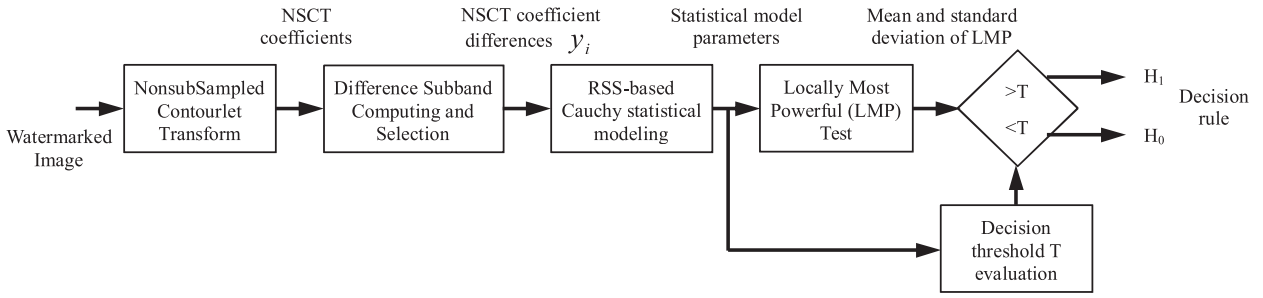
Fig. 6. The key components of the proposed locally most powerful (LMP) watermark detector.

the NSCT coefficient differences with RSS-based Cauchy statistical distribution, we propose a blind image watermark detector, namely locally most powerful (LMP) detector, by employing locally most powerful (LMP) test, which can effectively detect the watermark signal in the NSCT coefficient differences of a watermarked image. Fig. 6 shows the block diagram of our locally most powerful (LMP) watermark detector in NSCT domain using RSS-based Cauchy statistical distribution.

6.1. Locally most powerful (LMP) watermark detector

In the watermark detection process, the receiver needs to verify whether a specific watermark pattern is present or not in the received media, which can be regarded as a binary hypothesis test problem. Assuming that the alternative hypothesis H_1 and null hypothesis H_0 respectively means whether the NSCT coefficient differences are watermarked by pseudorandom sequence W or do not insert any watermark information, and the watermark detection is expressed as the following binary hypothesis test form

$$
\begin{aligned}
H_0 &: y_i = x_i \\
H_1 &: y_i = x_i(1 + \lambda \cdot w_l) = x_i + \underbrace{x_i \lambda w_l}_{w'_l} = x_i + w'_l
\end{aligned}
\tag{8}
$$

where x_i and y_i denote the NSCT coefficient differences of the selected subband of the original image and watermarked ones, respectively, w_l represent the pseudo-random watermark sequence, and λ is the watermark embedding strength.

It is well known from detection theory that, a locally most powerful (or locally optimal, LO) test is optimal for non-Gaussian weak signals in the sense of minimizing detection errors. Because authentication watermarks are almost always very weak signals, so a locally most powerful test is appropriate for designing a watermark detector. We assume that the NSCT coefficient differences has been modeled by RSS-based Cauchy distribution by presuming independence of the observations, and then we define the decision rule as the likelihood ratio given by

$$
\Lambda(Y) = \frac{P(Y|H_1)}{P(Y|H_0)} \underset{H_0}{\overset{H_1}{\underset{<}{>}}} \eta'
\tag{9}
$$

where $\Lambda(Y)$ is the likelihood ratio, and η' denotes the decision threshold. If $\Lambda(Y)$ is greater than decision threshold η', the alternative hypothesis H_1 exists, whereas the null hypothesis H_0 exists. Because the above likelihood ratio test contains several multiplication items, and the probability value of each multiplication item is between 0 and 1, so the final probability value is sometimes very small, even the underflow occurs. To solve this problem, we take the log of both sides in (9), and obtain the log-likelihood ratio, which does not affect the monotonicity. Because multiplication operation becomes addition operation, the computational complexity is reduced. So in practice, the log-likelihood ratio is usually preferred to perform hypothesis testing. The log-likelihood ratio is clearly a superposition of N statistically independent random variables with finite mean and variance [25]. Therefore, it is more convenient to use log-likelihood ratio. The log-likelihood ratio is simply defined as the natural logarithm of the likelihood ratio, hence the decision formula rule becomes

$$
l(\bar{Y}) = \ln \Lambda(Y) = \sum_{i=1}^{N} \ln \frac{P_Y(y_i|H_1)}{P_Y(y_i|H_0)} = \sum_{i=1}^{N} \ln \frac{P_x(y_i - w'_l)}{P_x(y_i)} \underset{H_0}{\overset{H_1}{\underset{<}{>}}} \eta
\tag{10}
$$

where $\ln \Lambda(Y)$ is the log-likelihood ratio, $\eta = \ln(\eta')$.

The watermark detector is supposed to choose between the alternative hypothesis H_1 and null hypothesis H_0 based on the received image Y. In this case, if $\ln \Lambda(Y) > \eta$, the alternative hypothesis H_1 is accepted; otherwise, the null hypothesis H_0 is accepted. For the log-likelihood ratio in (10), the following Taylor series approximation can be obtained by using the locally most powerful test

$$
l(y_i)|_{w'_l} = l(y_i)|_{w'_l=0} + \frac{\partial l(y_i)}{\partial w'_l}\Bigg|_{w'_l=0} \cdot w'_l + o(w'_l) \cong g_{LO}(y_i) \cdot w'_l + o(|w'_l|) = g_{LO}(x_i) \cdot w'_l
\tag{11}
$$

where $g_{LO}(x)$ is the "locally optimum non-linearity" [6,7]. We have proved that the RSS-based Cauchy statistical model can more accurately fit the NSCT coefficient differences distribution in Section 4.2, so the locally optimum non-linearity formula is derived by combine with RSS-based Cauchy distribution as follows

$$g_{LO}(x) = -\frac{f'_X(x)}{f_X(x)} = \frac{2(x - \delta)}{(x - \delta)^2 + \gamma^2} \tag{12}$$

where δ and γ are the location parameter and shape parameter of the RSS-based Cauchy distribution, respectively, and x is the input NSCT coefficient differences.

Substituting (12) into (11), the final detector expression can be written as

$$l(g_{LO}(\bar{Y})) = \sum_N g_{LO}(y_i) \cdot w'_l = \sum_N \frac{2y_i w_l(y_i - \delta)}{(y_i - \delta)^2 + \gamma^2} \tag{13}$$

where $\bar{Y}$ is the vector of N NSCT coefficient differences which are input to the locally optimal non-linearity, and $g_{LO}(\bar{Y})$ denotes its output.

It is clear from (13) that the log-likelihood ratio can be seen as a superposition of N statistically independent random variables. In view of this, according to the central limit theorem (CLT), we can approximate the distribution of the log-likelihood ratio test by a Gaussian distribution under each hypothesis. So, we can estimate the mean and variance of each Gaussian distribution under the two assumptions H_0 and H_1 from the empirical data. We assume that the digital watermark is a pseudorandom sequence, which takes the values of $+1$ and -1 with equal probabilities $1/2$. Thus the mean m_0 under the null hypotheses H_0 is given by

$$m_0 = E_s \left[\sum_N \frac{2y_i w_l(y_i - \delta)}{(y_i - \delta)^2 + \gamma^2} \right] = 0 \tag{14}$$

Under the alternative hypothesis H_1, the mean m_1 is given by

$$m_1 = E_s \left[\sum_N \frac{2(x_i + w'_l - \delta) \cdot y_i w_l}{(x_i + w'_l - \delta)^2 + \gamma^2} \right] = \sum_N \left(\frac{(x_i + \lambda x_i - \delta) \cdot x_i}{(x_i + \lambda x_i - \delta)^2 + \gamma^2} - \frac{(x_i - \lambda x_i - \delta) \cdot x_i}{(x_i - \lambda x_i - \delta)^2 + \gamma^2} \right) \tag{15}$$

where we have $y_i = x_i + w'_l$. Then the formula (15) is simplified as follows

$$x_1 = \frac{(x_i + \lambda x_i - \delta) \cdot x_i}{(x_i + \lambda x_i - \delta)^2 + \gamma^2} \qquad x_2 = \frac{(x_i - \lambda x_i - \delta) \cdot x_i}{(x_i - \lambda x_i - \delta)^2 + \gamma^2} \tag{16}$$

Therefore, (16) can be simplified as follows

$$m_1 = \sum_N (x_1 - x_2) \tag{17}$$

Then the variance σ_0^2 under the null hypotheses H_0 is given by

$$\sigma_0^2 = E_s \left[\left(\sum_i^N \frac{2(y_i - \delta) \cdot y_i w_l}{(y_i - \delta)^2 + \gamma^2} \right)^2 \right] = \sum_i^N E_s \left[\left(\frac{2(y_i - \delta) \cdot y_i w_l}{(y_i - \delta)^2 + \gamma^2} \right)^2 \right]$$

$$+ \sum_l \sum_{l \neq i} E_s \left[\frac{4(y_i - \delta) \cdot y_i w_l(y_l - \delta) \cdot y_l w_l}{((y_i - \delta)^2 + \gamma^2)((y_l - \delta)^2 + \gamma^2)} \right] = 4 \sum_i^N \frac{(y_i - \delta)^2 \cdot y_i^2}{\left[(y_i - \delta)^2 + \gamma^2 \right]^2} \tag{18}$$

When the watermark information exist, then the formula is given by

$$l(g_{LO}(\bar{Y})|H_1) - m_1 = \frac{1}{2\sigma^2} \times \sum_N \left(\frac{4(x_i + w'_l - \delta) \cdot y_i w_l}{(x_i + w'_l - \delta)^2 + \gamma^2} - 2x_1 + 2x_2 \right) \tag{19}$$

where σ represent the variance of the watermark parameters estimation. We substitute formula (17) into (19), the variance σ_1^2 can be obtained as

$$\sigma_1^2 = E_s \left[\sum_N (x_1 + x_2)^2 \right] = \left[\frac{2(y_i - \delta)}{(y_i - \delta)^2 + \gamma^2} \cdot y_i w_l - (x_1 - x_2) \right]^2 \tag{20}$$

6.2. Performance analysis

The work quality of the derived watermark detector can be analyzed theoretically by connecting the probability of false alarm (P_{fa}) rate and the probability of detection (P_{det}) rate [25]. Generally, a good watermark detection scheme should

reduce the P_{fa} and increase P_{det} as much as possible. The receiver operating characteristic (ROC) curve is a compromise method between the P_{fa} and P_{det}. In this paper, the ROC curve is employed to evaluate the performance of the designed LMP watermark detector. Having obtained the variance and mean based on log-likelihood ratio by a Gaussian distribution under each hypothesis, so the false alarm probability P_{fa} can be estimated as follows

$$P_{fa} = p(\Lambda(Y)|H_0 > \eta) = Q\left(\frac{\eta - m_0}{\sigma_0}\right) \tag{21}$$

where m_0 and σ_0^2 are the mean and variance of $\Lambda(Y)$ under null hypothesis H_0, respectively. $Q(x)$ is expressed as $Q(x) = \frac{1}{\sqrt{2\pi}} \int_x^{+\infty} e^{-t^2/2} dt$.

The detection probability P_{det} of the watermark detector is computed by

$$P_{det} = p(\Lambda(Y)|H_1 > \eta) = Q\left(\frac{\eta - m_1}{\sigma_1}\right) \tag{22}$$

where m_1 and σ_1^2 are the mean and variance of $\Lambda(Y)$ under alternative hypothesis H_1, respectively.

When the false alarm probability P_{fa} is given, the decision threshold for watermark detection can be calculated as follows

$$\eta = m_0 + \sigma_0 Q^{-1}(P_{fa}) \tag{23}$$

The relationship between the P_{fa} and P_{det} can be found through a predefined threshold to derive the ROC curve. The formula can be obtained as follows

$$P_{det} = Q\left(\frac{\sigma_0}{\sigma 1} Q^{-1}(P_{fa}) - \frac{m_1 - m_0}{\sigma_1}\right) \tag{24}$$

7. Experimental results

In this section, we use three evaluation metrics, including watermark-to-document ratio (WDR), receiver operating characteristics (ROC) curves, and AUROC (the area under the ROC), to examine the detection performance based on given testing results. Here, WDR is used to describe the embedding power of the watermark by the power ratio between watermarks and the unmarked transform coefficients. ROC is generated by relating the probability of false alarm P_{fa} and the probability of detection P_{det}. For a predefined rate of false alarm, the reliability of detector requires maintaining a high probability of detection. AUROC for the P_{fa} range [0–1] is used to quantify the performance of the detector at low false alarm rates. And the total area under the ROC curve is calculated to quantify the overall performance of the detector. In our simulation, the experimental ROC curves and AUROC values are tested by averaging over 10 runs with 1024 different pseudorandom sequences as the watermark bits.

The test images used in this paper are $512 \times 512 \times 8$ bits standard grayscale image from Computer Vision Group Test Images database [33]. Experiment results are achieved in MATLAB R2011a on an Intel(R) Xeon E5-16030 CPU@2.80 GHz processor. In order to achieve better performance of the designed detector, we embedded the watermark into the robust NSCT coefficient differences, where the pseudorandom sequence is employed as watermark signal. Because the RSS-based Cauchy distribution can reflect effectively the statistical characteristics of the robust NSCT coefficient differences, the proposed detection method have better work performance. In view of this, the main process of detector construction is summarized as follows: (1) Perform two-level NSCT on the image, wherein four directions are used in each level; (2) Calculate the difference subbands and the highest energy difference subband is selected to embed the watermark information; (3) Analyze the statistical properties of watermarked coefficient differences and estimate the parameters by using the RSS method; (4) The watermark detection is formulated as the binary detection problem, and LMP detector is constructed by employing RSS-based Cauchy distribution; (5) The mean and variance of closed-form statistic strategies are derived under the hypothesis to obtain the ROC curves of the proposed detector.

7.1. Imperceptibility evaluation

In order to evaluate the imperceptibility of digital watermark, the signal-to-noise ratio (PSNR) measure is employed in this paper. PSNR is an objective criterion, which is always used to evaluate image quality. According to theory [15], when the PSNR value of the watermarked image is larger than 38 dB, the human eyes cannot detect the difference between the original image and the watermarked one. So PSNR > 38 dB can be used as a criterion to judge the quality of watermark embedding.

Fig. 7 is the experimental result of applying our watermarking algorithm for data embedding in original host images Lena, Barbara, Peppers, Airplane, and Baboon. Fig. 7(a)–(e) show the original host images. Fig. 7(f)–(j) report the watermarked images with WDR = −64 dB, and corresponding PSNR values. Fig. 7(k)–(o) are the absolute differences between origin host image and watermarked one, multiplied by 20 for better display. From the Fig. 7, we can know that the proposed NSCT coefficient differences based multiplicative watermarking scheme provides better imperceptibility.
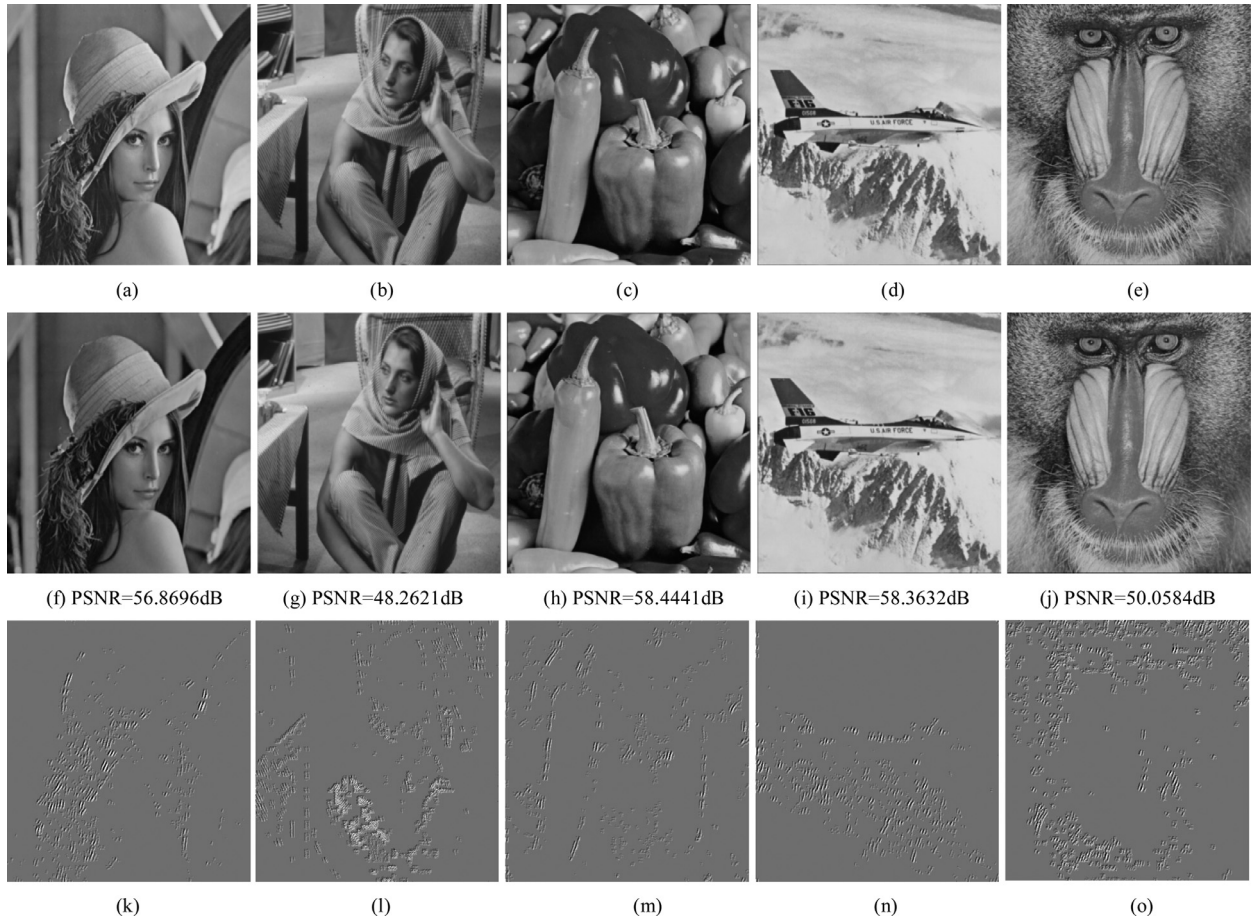
Fig. 7. The watermark embedding examples by using our approach: (a)–(e) The original host images, (f)–(j) The watermarked images, (k)–(o) The absolute difference between original images and the watermarked ones.

Table 3
AUROC values under various attacks for different images.

Images	Attack types							
	No attack	AWGN ($\sigma_n^2=100$)	Median filtering [4×4]	Gaussian filtering [3×3]	Rotate (10°)	JPEG (Q=45%)	Intensity scaling scaled to half value	Cropping rectangular
Lena	0.9613	0.9609	0.7685	0.9593	0.6574	0.9596	0.8860	0.9564
Barbara	0.9791	0.9765	0.9289	0.9441	0.8564	0.9742	0.9645	0.9769
Peppers	0.7946	0.7929	0.6697	0.7644	0.5662	0.7056	0.6666	0.7924
Airplane	0.9849	0.9621	0.9221	0.9887	0.7892	0.9889	0.8772	0.9837
Baboon	0.9990	0.9933	0.9807	0.9993	0.9753	0.9972	0.9576	0.9990

7.2. Performance evaluation of the proposed detector

Here, we evaluate the quality of watermark detector from two aspects: watermark detection accuracy and robustness. We implement the proposed LMP watermark detector, and compute the AUROC area for different test images ("Lena," "Barbara," "Peppers," "Baboon," "Airplane") under different attacks with WDR = −64 dB. Attack types include AWGN, Median filtering with [4 × 4], Gaussian filtering with [3 × 3], Rotate, Scaling, Cropping, as well as JPEG Compression. Table 3 reports the AUROC results for the proposed watermark detector under various attacks.

Fig. 8 shows the detector response for image Barbara and Lena images under the JPEG compression, where for each quality factors increase varying from 1 to 100, the detector response for 1024 randomly generated watermarks has been measured. Fig. 9 shows the detector response for the Barbara and Lena images with windows of size 3 × 3, 5 × 5 and 7 × 7 for the median filter. Fig. 10 gives the ROC curves for Lena, Barbara, Peppers, Baboon and Airplane images with $\sigma_n^2 =$
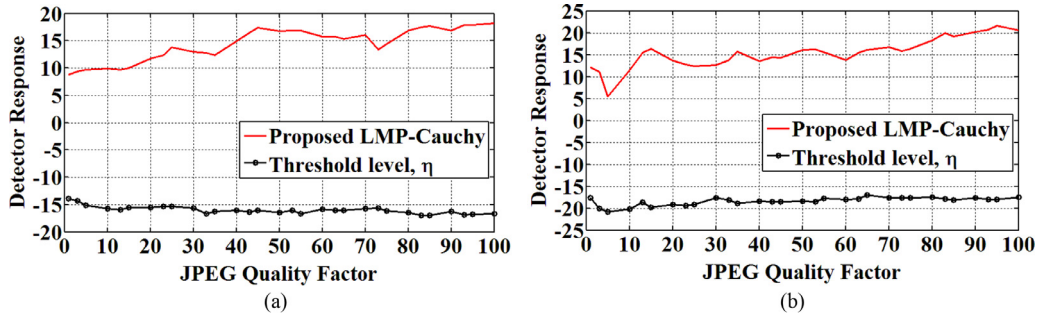
Fig. 8. The detector response under JPEG compression for images Barbara and Lena: (a) Barbara, and (b) Lena, where the quality factors varying from 1 to 100 with WDR = −40 dB.
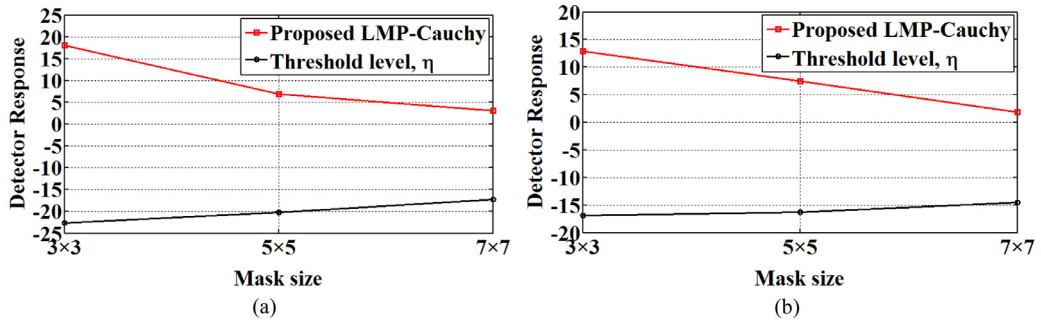

Fig. 9. The detector response for standard images Barbara and Lena: (a) Barbara, and (b) Lena, under median filtering with windows of size of 3×3, 5×5 and 7×7, WDR = −40 dB.
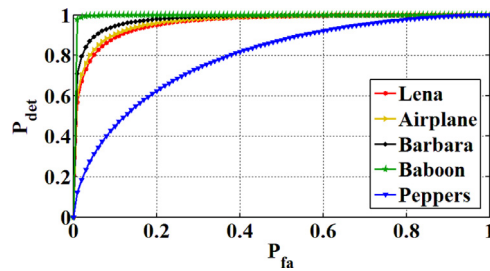

Fig. 10. The ROC curves for different test images with WDR = −64 dB under $\sigma_n^2 = 100$ AWGN attack.
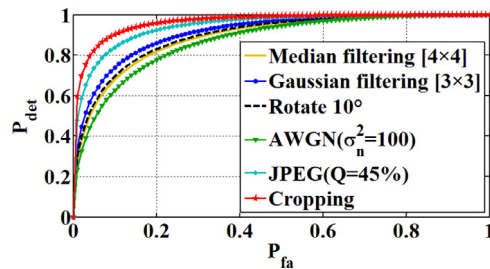

Fig. 11. The average ROC curves under various types of attacks with WDR = −64 dB.

100AWGN attack and WDR = −64 dB. Fig. 11 gives the average ROC curves under different types attacks with WDR = −64 dB. We also compute the average CPU time of the proposed LMP detector for different test images, and the average CPU time is 0.487 s. We can see from the above experimental results, the proposed LMP watermark detectors have lower computational complexity, and better robustness and detection rate.
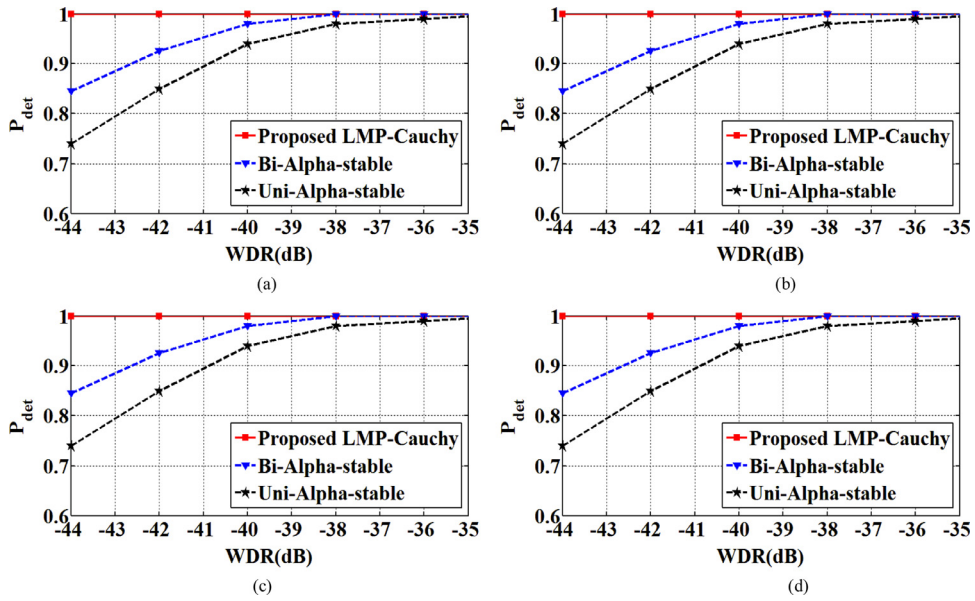
Fig. 12. The ROC curves of the proposed detector and alpha-stable distribution based watermark detector [25] for different WDR values: (a) Lena, (b) Barbara, (c) Peppers, and (d) Airplane.
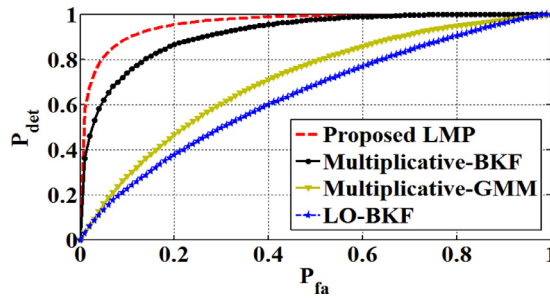

Fig. 13. The average ROC curves of the proposed LMP detector and some other statistical detector with WDR = −64 dB.

Table 4
AUROC values for different WDR with no attack.

WDR(dB)	GMM [2]	Multiplicative BKF [23]	LO-BKF [7]	Proposed LMP detector
−62	0.7085	0.9512	0.7166	**0.9983**
−64	0.6918	0.9067	0.6358	**0.9791**
−66	0.6836	0.8516	0.5684	**0.9252**
−68	0.6606	0.7986	0.5403	**0.8630**

7.3. Comparison with other methods

In this section, we compare the performance of the designed LMP detector with other statistical watermark detectors [2,7,23,25]. Fig. 12 provides the ROC curves of the proposed detector and alpha-stable distribution based watermark detector [25], for test images Lena, Barbara, Peppers, and Airplane, in the case of no attack.

Fig. 13 shows the average ROC curves for the proposed detector and some other statistical detectors, which includes Multiplicative-BKF [23], Multiplicative-GMM [2], and additive LO-BKF [7] methods.

Table 4 shows the AUROC values for Barbara image in the case of no attack. The AUROC values for Barbara under the JPEG compression (QF=55%) can be shown in Table 5. Table 6 provides the AUROC values for Barbara under the cropping attack.

In order to further evaluate the detection performance of the proposed scheme, we also compare the proposed detector to other statistical watermark detectors [2,7,23], and obtain the CPU times of the various detectors by averaging a number of test images and watermark sequences. Table 7 gives the CPU times averaged over a number of test images and watermark

Table 5
AUROC values for different WDR under JPEG compression (QF=55%).

WDR (dB)	GMM [2]	Multiplicative BKF [23]	LO-BKF [7]	Proposed LMP detector
−58	0.7366	0.9738	0.8706	**0.9958**
−60	0.7346	0.9399	0.8162	**0.9774**
−62	0.7212	0.8871	0.7235	**0.9398**

Table 6
AUROC values for different WDR under cropping attack.

WDR (dB)	GMM [2]	Multiplicative BKF [23]	LO-BKF [7]	Proposed LMP detector
−56	0.7573	0.9488	0.9389	**0.9950**
−58	0.7493	0.9052	0.8986	**0.9937**
−60	0.7424	0.8515	0.8697	**0.9890**

Table 7
The average detection time for various statistical watermark detectors.

	Scheme [2]	Multiplicative BKF [23]	LO-BKF [7]	Proposed LMP detector
CPU time (seconds)	0.634	0.507	0.962	**0.487**

sequences. It is observed from the Figs. 12 to 13 and Tables 4 to 7 that the proposed watermark detector provides the highest detection rate with comparable or lower computational time.

From above simulation experimental results, it is clear that (1) the proposed detector has the best rates of detection as compared to the other statistical watermark detectors, and similar experimental results can be observed from other test images. The reason for more accurate detection rates is that the RSS-based Cauchy distribution is introduced to capture effectively the statistical behavior of NSCT coefficient differences, and the locally most powerful test criterion is utilized to minimize the non-Gaussian weak watermark signals detection errors. (2) the provided detector is much more robust than other statistical watermark detectors. This is because that we employ the robust NSCT coefficient differences to insert watermark signal and design watermark detector.

It should be noted that, the proposed technique can also deal with color images, because it can be directly applied on the luminance component or three color channels of color images. However, it has been shown that the performance of such a method for color images is not satisfactory, for it ignores the important dependencies between RGB color channels. Future research may focus on taking into account the interchannel dependencies between RGB channels and various strong dependencies of the transform coefficients of color images by employing the vector based statistical model.

8. Conclusion

In this paper, we proposed a novel statistical model image watermarking algorithm based on robust NSCT coefficient differences. NSCT can accurately calculate the contourlet coefficients based on a multiresolution analysis, and also can achieve the optimum approximation rate for piecewise smooth functions with discontinuities. According to the inter-scale dependency between NSCT coefficients, we computed the NSCT coefficient differences and investigated their robustness by subjective visual error and objective mean squared error (MSE) terms. We inserted the watermark signal into the high-energic subband by modulating the robust NSCT coefficient differences. We analyzed the statistical properties of NSCT coefficient differences, and modeled accurately the NSCT coefficient differences with RSS-based Cauchy distribution. And furthermore, we developed a blind locally optimum NSCT domain multiplicative detector based on RSS-based Cauchy statistical distribution and locally most powerful test criterion, which is optimal for non-Gaussian weak watermark signals in the sense of minimizing detection errors. Also, we employed the statistical model to derive the closed-form expressions for the watermark detector. We evaluated the performance of the designed NSCT domain watermark detector in detail by conducting several simulation experiments, and the experimental results have shown that the detection performance of the proposed detector is superior to that of the state-of-the-art methods recently provided in the literature, in terms of the imperceptibility and robustness well as the efficacy.

It is worthing to point out that, the proposed approach can also deal with color images by using directly the luminance component or three color channels of color images. However, it has been shown that the performance of such an approach for color images is not satisfactory, for it ignores the important dependencies between RGB color channels. Future research may focus on taking into account the interchannel dependencies between RGB channels and various strong dependencies of the transform coefficients of color images by employing the vector based statistical model.

Conflict of interest

None.

Acknowledgments

References

[1] B. Ahmederahgi, F. Kurugollu, P. Milligan, A. Bouridane, Spread spectrum image watermarking based on the discrete shearlet transform, in: European Workshop on Visual Information Processing, 2013, pp. 178–183.

[2] M. Amirmazlaghani, M. Rezghi, H Amindavar, A novel robust scaling image watermarking scheme based on gaussian mixture model, Expert Syst. Appl. 42 (4) (2015) 1960–1971.

[3] M. Amini, Wavelet Domain Watermark Detection and Extraction Using the Vector-based Hidden Markov Model, Concordia University, 2016.

[4] M. Amini, M. O. Ahmad, M.N.S Swamy, A new locally optimum watermark detection using vector-based hidden markov model in wavelet domain, Signal Process. 137 (2017) 213–222.

[5] M. Barni, F. Mauro, A. De. Rosa, A. Piva, A new decoder for the optimum recovery of nonadditive watermarks, IEEE Trans. Image Process. 10 (5) (2001) 755–766.

[6] A. Briassouli, M. G. Strintzis, Locally optimum nonlinearities for DCT watermark detection, IEEE Trans. Image Process. 13 (12) (2004) 1604–1617.

[7] Y. Bian, S. Liang, Locally optimal detection of image watermarks in the wavelet domain using Bessel k form distribution, IEEE Trans. Image Process. 22 (6) (2013) 2372–2384.

[8] Y. Bian, S. Liang, Image watermark detection in the wavelet domain using Bessel k densities, IET Image Proc. 7 (4) (2013) 281–289.

[9] H. Bi, Y. Liu, M. Wu, Y. Ge, NSCT domain additive watermark detection using RAO hypothesis test and cauchy distribution, Math. Probl. Eng. 2016 (2016) 18 4065215.

[10] P. Bhinder, K. Singh, N. Jindal, Image-adaptive watermarking using maximum likelihood decoder for medical images, Multimed. Tools Appl. 3 (2018) 1–26.

[11] A. L.Da Cunha, J. Zhou, M. N. Do, The nonsubsampled contourlet transform: theory, design, and applications, IEEE Trans. Image Process. 15 (10) (2006) 3089–3101.

[12] L. Dong, Q. Yan, Y. Lv, S. Deng, Full band watermarking in DCT domain with Weibull model, Multimed. Tools Appl. 76 (2) (2017) 1983–2000.

[13] C. Deng, H. Zhu, S. Wang, Curvelet domain watermark detection using alpha-stable models, in: International Conference on Information Assurance and Security, 1, 2009, pp. 313–316.

[14] S. Etemad, M. Amirmazlaghani, A new multiplicative watermark detector in the Contourlet domain using t Location-Scale distribution, Pattern Recognit. 77 (2018) 99–112.

[15] S.A.M Gilani, I. Kostopoulos, A.N. Skodras, Color image-adaptive watermarking, in: Proceedings of the 14th International Conference on Digital Signal Processing, Santorini, Greece, 2002, pp. 721–724.

[16] T. Huynh-The, O. Banos, S. Lee, Y. Yoon, T. Le-Tien, Improving digital image watermarking by means of optimal channel selection, Expert Syst. Appl. 62 (15) (2016) 177–189.

[17] T. Huynh-The, C.H. Hua, N.A. Tu, T. Hur, J. Bang, D. Kim, M.B. Amin, B.H. Kang, H. Seung, S. Lee, Selective bit embedding scheme for robust blind color image watermarking, Inf. Sci. 426 (2018) 1–18.

[18] R. Kwitt, P. Meerwald, A. Uhl, Lightweight detection of additive watermarking in the DWT-domain, IEEE Trans. Image Process. 20 (2) (2011) 474–484.

[19] R. Kwitt, P. Meerwald, A. Uhl, Efficient detection of additive watermarking in the DWT-domain, in: European Signal Processing Conference, 2009, pp. 2072–2076.

[20] N.K. Kalantari, S.M. Ahadi, M. Vafadust, A robust image watermarking in the Ridgelet domain using universally optimum decoder, IEEE Trans. Circuits Syst. Video Technol. 20 (3) (2010) 396–406.

[21] A. Khawne, B. Attachoo, K. Hamamoto, Optimum watermark detection of ultrasonic echo medical images, IEEJ Trans. Electr. Electr. Eng. 10 (2) (2015) 149–156.

[22] A.F. Qasim, F. Meziane, R. Aspin, Digital watermarking: applicability for developing trust in medical imaging workflows state of the art review, Comput. Sci. Rev. 27 (2018) 45–60.

[23] M. Rabizadeh, M. Amirmazlaghani, M. Ahmadian-Attari, A new detector for contourlet domain multiplicative image watermarking using Bessel K form distribution, J. Visual Commun. Image Represent. 40 (2016) 324–334.

[24] S.M.M. Rahman, M.O. Ahmad, M.N.S. Swamy, A new statistical detector for DWT-based additive image watermarking using the Gauss-Hermite expansion, IEEE Trans. Image Process. 18 (8) (2009) 1782–1796.

[25] H. Sadreazami, M.O. Ahmad, M.N.S. Swamy, A study of multiplicative watermark detection in the Contourlet domain using alpha-stable distributions, IEEE Trans. Image Process. 23 (10) (2014) 4348–4360.

[26] H. Sadreazami, M.O. Ahmad, M.N.S. Swamy, Multiplicative watermark decoder in contourlet domain using the normal inverse Gaussian distribution, IEEE Trans. Multimed. 18 (2) (2016) 196–207.

[27] H. Sadreazami, M.O. Ahmad, M.N.S. Swamy, A robust multiplicative watermark detector for color images in sparse domain, IEEE Trans. Circuits Syst. II 62 (12) (2015) 1159–1163.

[28] V. Santhi, Adaptive color image watermarking scheme using Weibull distribution, in: N. Dey, V. Santhi (Eds.), Intelligent Techniques in Signal Processing for Multimedia Security, Cham, Studies in Computational Intelligence, Springer, 2017, pp. 453–468.

[29] J. Wang, G. Liu, Y. Dai, J. Sun, Z. Wang, S. Lian, Locally optimum detection for barni's multiplicative watermarking in DWT domain, Signal Process. 88 (1) (2008) 117–130.

[30] X. Wang, Y. Liu, H. Xu, A. Wang, H. Yang, Blind optimum detector for robust image watermarking in nonsubsampled Shearlet domain, Inf. Sci. 372 (2016) 634–654.

[31] X. Wang, S. Zhang, L. Wang, H. Yang, P. Niu, Locally optimum image watermark decoder by modeling NSCT domain difference coefficients with vector based Cauchy distribution, J. Visual Commun. Image Represent. 62 (2019) 309–329.

[32] O.M. Yousef, S.A. Al-Subh, Estimation of gumbel parameters under ranked set sampling, J. Mod. Appl. Stat. Methods 13 (2) (2014) 432–443.

[33] Available: http://decsai.ugr.es/cvg/dbimagenes/index.php .